Journal of Materials Chemistry

Cite this: *J. Mater. Chem.*, 2012, **22**, 5900

www.rsc.org/materials

FEATURE ARTICLE

Unconventional methods for fabricating nanostructures toward high-fidelity sensors

Su Yeon Lee, Hwan Chul Jeon and Seung-Man Yang*

Received 13th December 2011, Accepted 26th January 2012
DOI: 10.1039/c2jm16568f

Plasmonic materials fabricated from precisely controlled metal nanostructures provide promising platforms for developing high-sensitivity sensing devices, such as pH sensors, organic vapor sensors, and other chemical sensors. Over the past several decades, a number of unconventional methods for preparing localized surface plasmon resonance (LSPR)-based metal nanostructures have been developed in an effort to design high-fidelity sensors. Recent advances in plasmon-based optical sensors based on plasmonic nanostructures have made remarkable progress in overcoming the constraints of conventional optical sensors in terms of providing tunability, improved sensitivity, and good fidelity. In this review, we highlight the current state of the art in this field with an emphasis on the fabrication of plasmonic materials using unconventional methods and their demonstrated applications. We describe the remarkable achievements that have improved the performance of sensors for certain sensing systems. Finally, we present a perspective on the future development of LSPR sensors, including a discussion of the advances needed to elevate sensor performance to a level required for practical devices in the laboratory and in medical diagnostics.

1. Introduction

Surface plasmons (SPs) are coherent oscillations of electromagnetic (EM) waves and surface-bound charges that can propagate along metal–dielectric interfaces.[1] SPs are classified into two types: propagating surface plasmons, that is, surface plasmon polaritons (SPPs),[1,2] and localized surface plasmon resonances (LSPRs).[3,4] In general, both SPPs and LSPRs contribute to the optical characteristics of a nanostructure. Control over the properties of SPs *via* adjustments to the geometric parameters of the nanostructures is a growing area of focus in plasmonic research. SPs respond to changes in the local refractive index (RI) with high sensitivity, which supports the potential for label-free plasmonic detection of biomolecular binding. For example, surface plasmon resonance (SPR) measurements are commonly used to identify and analyze chemical and biological analytes without the requirement for phosphorescent or fluorescent labels.[4] Standard SPR methods

National Creative Research Initiative Center for Integrated Optofluidic Systems and Department of Chemical and Biomolecular Engineering, KAIST, Daejeon, 305-701, Korea. E-mail: smyang@kaist.ac.kr; Fax: +82-42-350-5962; Tel: +82-42-350-3922

Su Yeon Lee

Su Yeon Lee received his BS degree in Chemical Engineering from Yonsei University in 2005, and MS (2007) and PhD (2011) in Chemical and Biomolecular Engineering from KAIST. Currently, he is working with Prof. Seung-Man Yang as a post-doctoral researcher at KAIST. His major research interests lie in plasmonic nanostructures for biomolecular sensors as well as development of optofluidic sensing platforms.

Hwan Chul Jeon

Hwan Chul Jeon is a PhD candidate in Chemical and Biomolecular Engineering at KAIST. He received his BS degree in Chemical Engineering from Yonsei University in 2009. During three years at KAIST, he worked on nanopatterning via *prism holographic lithography. Currently, his main research interests lie in plasmonic nanostructures for biomolecular detection.*

utilize the properties of SPs in the SPP class. In a typical optical configuration that employs these propagating plasmons, such as the Kretschmann configuration, a prism couples light to the SPs on the surface of a 50 nm thick gold film.[5,6] With accurate alignment, the incident light undergoes total internal reflection on the inner surface of the prism. At the SPR angle, an evanescent wave penetrates the gold thin film and excites SPs at the metal–dielectric interface. The SPR angle is sensitive to several parameters, including the thickness of the gold film, the wavelength of light, the RI of the medium in contact with the metallic surface, and the physical and optical properties of the prism.

The complexities of high numerical optics, however, makes it difficult to integrate these techniques into portable low-cost devices and high-throughput systems.[7] These restrictions can be overcome through the use of metallic nanostructures, such as metallic nanoparticles (NPs), nanohole or nanowell arrays in metal films, and other structures that provide EM field localization.[3,8–11] These metallic nanostructures give rise to LSPRs that can be manipulated by precisely controlling the shape and size of the metal nanostructures and the local dielectric environment. In contrast to propagating SPPs, nonpropagating LSPRs are confined to structures and can be excited. Thus, plasmonic nanostructures make it possible to probe systems with a higher spatial resolution than would be possible using propagating SPPs.[12,13] This advantage has been exploited for label-free optical sensing in systems in which RI changes near or on metallic nanostructures are used to detect binding events.

A variety of methods for fabricating metal NPs have been proposed, yielding random or periodic arrays of nanohole (nanowell) structures in metal films; however, these methods usually require complicated and time-consuming techniques, such as focused ion-beam (FIB) milling,[14,15] and electron beam lithography (EBL).[16–19] These techniques only permit the fabrication of small areas of holes in metal films *via* a serial process, and they are ineffective for patterning nanostructures over large areas. As an alternative method, colloidal lithography (CL), which uses a hexagonally close-packed monolayer of colloidal particles on a surface as an etching or deposition mask for the fabrication of periodic arrays of metal nanostructures, has been proposed.[20–23] This unconventional method allows the fabrication of defect-free plasmonic nanostructures 10–100 μm^2 in area, with controlled geometry, to yield metallic nanostructures that exhibit plasmonic properties. More recent reports have described the fabrication of plasmonic nanostructures over large areas using soft nanoimprint lithography and soft interference lithography (SIL). In these methods, a topographically patterned poly(dimethylsiloxane) (PDMS) stamp was used to emboss a thin UV-curable polyurethane film, or a stamp was used as a phase mask for phase-shifting photolithography. A metal film can be deposited on the resulting structures to create high-resolution plasmonic nanostructures at relatively low cost. Unconventional methods for fabricating plasmonic nanostructure templates have been proposed based on several techniques: interference lithography (IL), block copolymers (BCPs), and porous alumina templates. These techniques are facile, cost-effective, and applicable to large-area manufacturing.

Three main approaches are available for SP-based chemical sensing. The first approach relies on the dependence of SPR on the dielectric constant at the metal–dielectric interface. The SPR is sensitive to changes in the RI caused by molecular adsorption.[24] In this approach, changes in the dielectric environment at the surface of a flat or periodically structured metal film can shift the observed SPR resonance, which can be measured using wavelength-dependent absorption, angular-dependent absorption, or intensity measurements. The second approach investigates the red shift in the LSPR absorption of metallic NPs due to NP aggregation.[25] In particular, plasmonic metallic nanostructures have been proposed as novel materials for chemical and biomolecular detection due to the exceptional characteristics of metal nanostructures such as LSPRs and SERS. LSPR properties caused by 2D metallic nanostructures can be characterized simply by measuring the absorption, transmission, or reflectance spectra. LSPR from 2D metal nanopatterns under excitation by EM radiation of a certain wavelength generate a collective oscillation of conduction electrons at surfaces. The third approach utilizes subwavelength EM field localization related to SP excitation, which enhances spectroscopic measurements, such as surface-enhanced Raman scattering (SERS)[26–31] and surface-enhanced fluorescence spectroscopy (SEFS).[32–34] A roughened noble metal surface can be used as a SERS substrates by coupling incident light to SPs with a high enhancement factor (EF). Recent reports have described the preparation of precisely controlled metal nanoparticles,[29,35] nanoshells,[31] nanoscale holes,[17,36] and voids[30,37] in metal films for use as SERS substrates. These metallic nanostructures can offer a more reliable performance, such as direct molecular identification and single-molecule detection.[38,39] Plasmonic photovoltaics are an exciting application of plasmonic materials.[40–46] Current photovoltaic technologies are based on crystalline silicon wafers typically 180–300 μm thick.[40] Although high-efficiency solar cells must exhibit a carrier diffusion length lower than the material thickness, this requirement is not met completely in thin solar cells. Recent approaches that combine solar cells with plasmonic nanostructures have emerged to concentrate and guide the light, leading to an increase in the absorption of incident light and a reduction in the semiconductor thickness.[40,47–49]

Seung-Man Yang

Seung-Man Yang received a PhD degree in Chemical Engineering from Caltech in 1985. Following this, he joined KAIST as a Professor in Chemical and Biomolecular Engineering. He has served KAIST as a director of the Computing Center, and a Department Chair. Currently, Professor Yang leads the Creative Research Initiative Center for Integrated Optofluidic Systems. His principal contributions have been in theories and experimental methods for fabricating ordered macrocrystalline structures, which can be applied as innovative functional nanoscopic materials such as optoelectronic devices and biosensors. He has authored over 200 peer-reviewed papers, and a number of books and patents in related areas.

In this article, we review the state-of-the-art plasmon-based sensing approaches with an emphasis on unconventional methods for fabricating metallic nanostructures that display LSPR properties. We outline the key strategies developed in recent years for high-sensitivity sensor applications. In Section 2, we discuss unconventional methods that have been used to create plasmonic nanostructures over large areas. Several examples of plasmonic nanostructure applications in chemical and biological sensing are presented in Section 3. Finally, we outline the future directions and outlook for the use of plasmonic nanostructures in high-sensitivity sensors in Section 4.

2. Fabrication of plasmonic nanostructures by unconventional methods

2.1 Colloidal lithography

Two-dimensional (2D) patterns with unique optical and chemical properties have attracted enormous interest due to wide applicability. Recently, several nanometre-scale fabrication methods have been investigated for the creation of novel nanostructures with distinct morphologies. Conventional fabrication methods for 2D nanopatterns include EBL, replica molding, FIB, multiple beam interferences, and CL techniques. Among these methods, CL, which uses colloidal particles as masks for etching or templates for the deposition of functional materials, has emerged as an unconventional method for fabricating plasmonic nanostructures.[50] CL presents several advantages for producing complex periodic nanostructures. CL is cost-effective because nanostructures have been produced using monodisperse colloidal particles or well-known techniques that are common to semiconductor manufacturing processes. 2D nanopatterns of the desired materials can be created simply by changing the deposition materials or modifying the colloidal surfaces with functional groups. Unique and exceptional structures with curved surfaces can be produced using a monolayer or multiple layers of spherical colloidal particles as templates. In addition, 2D or 3D patterns with complicated morphologies on the nanometre scale have larger surface areas than flat nanostructures, which increases the attachment of biomolecules for sensing applications.

2D colloidal particle arrays with low defects are required before subsequent fabrication procedures. Several methods are available for producing 2D colloidal crystals, including dip coating,[51] spin-coating,[52] lifting a colloid array from an air/liquid interface,[53] and electrophoretic assembly.[54] Among these methods, dip coating and spin-coating are the most widely used methods for CL because they create well-ordered colloidal arrays *via* a simple and inexpensive process that is applicable to large-area array formation. In some cases, a non-close-packed colloidal array can be fabricated by controlling the concentration of the colloidal dispersion, the solvent evaporation rate, and the substrate surface charge, which permit exploration of the properties of individual nanostructures fabricated by CL.[55] A variety of nanostructures have been manufactured using 2D colloidal arrays as masks for material deposition and etching.

Various 2D metal nanostructures prepared by CL have been used to detect biomolecules *via* plasmonic extinction measurements. Van Duyne and co-workers achieved significant improvements in LSPR biosensing methods using CL-fabricated metal nanoparticle arrays.[56–62] Fig. 1a illustrates the fabrication of silver nanotriangle arrays. Polymer nanospheres were coated on a substrate and self-assembled into a close-packed hexagonal array. Metal was then deposited on the 2D colloidal mask, and the mask was removed, leaving the silver nanotriangle arrays, as shown in Fig. 1b. This group also utilized electrochemistry to oxidize the nanotriangles, which modified their structures in a controlled manner. Fig. 1c shows the LSPR spectra and the corresponding atomic force microscopy (AFM) images of the silver nanotriangles during electrochemical oxidation. Prior to electrochemical oxidation, the Ag nanotriangle arrays exhibited an LSPR at 654 nm (Fig. 1c).[61] With each successive chronocoulometry experiment, the peak of the maximum extinction shifted to shorter wavelengths due to changes in the silver nanotriangle size and shape. AFM imaging was used to explore the geometry changes of the nanotriangle structures. After the initial electrochemical oxidation, the height of the nanotriangle structures did not change, whereas the 2D surface profile of the nanotriangle structures became smaller and rounder. The width was reduced from 126 ± 12 nm (Fig. 1d) to 87 ± 18 nm (Fig. 1f). The width variations of the nanotriangle structures led to shifts in the LSPR extinction spectra, from 654 to 506 nm. The extinction shifts appeared to result from the high EM field strength at the tips of the triangular nanostructures.

Lee and co-workers recently fabricated crescent-shaped nanoholes by using nanosphere lithography, as shown in Fig. 2a–c.[55,63–66] Using both systematic experimental and theoretical analysis, they characterized the optical properties of the crescent-shaped nanoholes and demonstrated the tunability of the crescent-shaped nanoholes by adjusting the geometric parameters. The experimental scattering profiles of the crescent-shaped nanoholes of different diameters were compared, which confirmed that a strong plasmonic response in the visible region

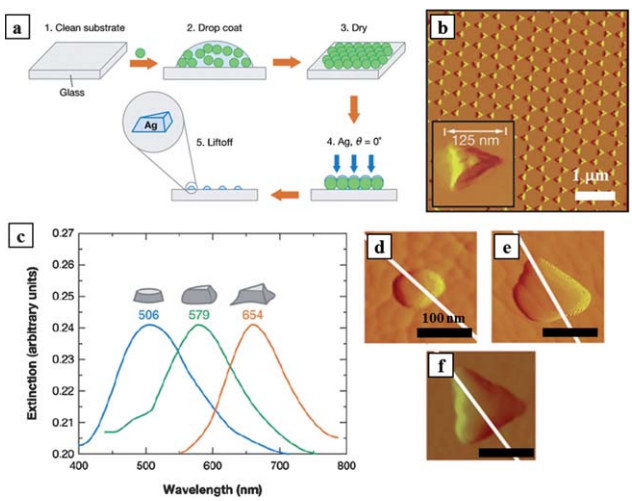

Fig. 1 (a) Schematic diagram of fabrication process of silver nanotriangle arrays. (b) AFM images of the resulting Ag triangular particles. (c) LSPR spectra of various sizes and shapes of Ag nanotriangle arrays fabricated by CL. (d–f) AFM images of nanotriangle structures after electrochemical oxidation. Scale bar in (b) and (d–f) are 1 mm, 100 nm, respectively. Reprinted with permission from ref. 61. Copyright 2007 Annual Reviews.

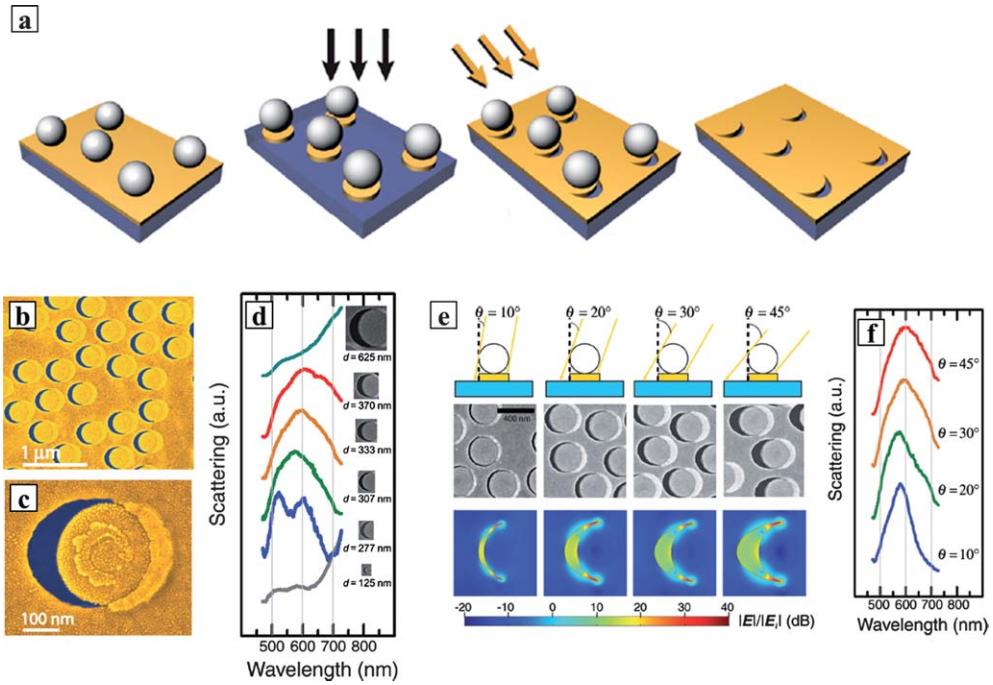

Fig. 2 (a) Schematic depiction of fabrication of crescent-shaped nanohole arrays. (b, c) SEM images of the resulting crescent-shaped nanohole arrays. (d) Experimental scattering of crescent-shaped nanohole with different diameters. (e) The shape variation of crescent-shaped nanohole by gold deposition angle. (f) Experimental scattering peak for the corresponding crescent-shaped nanohole structures. Reprinted with permission from ref. 55. Copyright 2009 American Chemical Society.

occurred for features 300 nm in diameter (Fig. 2d). A red shift in the scattering peak was obtained as the diameter of the crescent-shaped nanoholes increased. In addition, variations in the angle of gold deposition determined the shape of the crescent-shaped nanohole without varying its size, as shown in Fig. 2e. Although the shape of the nanohole changed considerably as the angle of gold deposition increased from 10° to 45°, the plasmon peak position did not affect the scattering spectra. The local electric field shown in Fig. 2f indicated that the strong plasmonic response of the crescent-shaped nanoholes was dominated by the sharp tips. Because the tip sharpness varied with the deposition angle, small changes in the plasmon peak wavelength were observed in the scattering spectra. Small deposition angles resulted in the creation of crescent-shaped nanoholes with sharp tips that produced high computed local field enhancements.

Recently, Heo *et al.* produced grail-shaped plasmonic nanostructures with plasmonic properties using CL for applications in which strong local field enhancements were required.[23,67] The plasmon resonance of the gold grails could be tuned over a broad spectral range, 600–2000 nm simply by varying the fabrication conditions. Fig. 3a illustrates the process of fabricating gold nanograil arrays, which include hexagonal closed-packing of silica particles, gold coating, and subsequent dry etching. Scanning electron microscopy (SEM) images of the fabricated gold nanograil structures are shown in Fig. 3b and c. The curved inner surfaces were molded by spherical silica particles. The experimental reflectance spectrum of the gold grail arrays is shown in Fig. 3d. In this spectrum, two pronounced dips were observed in the measured reflectance spectrum around 736 nm and 1754 nm. To investigate the origin of these dips, finite-difference time-domain (FDTD) simulations were performed using structural

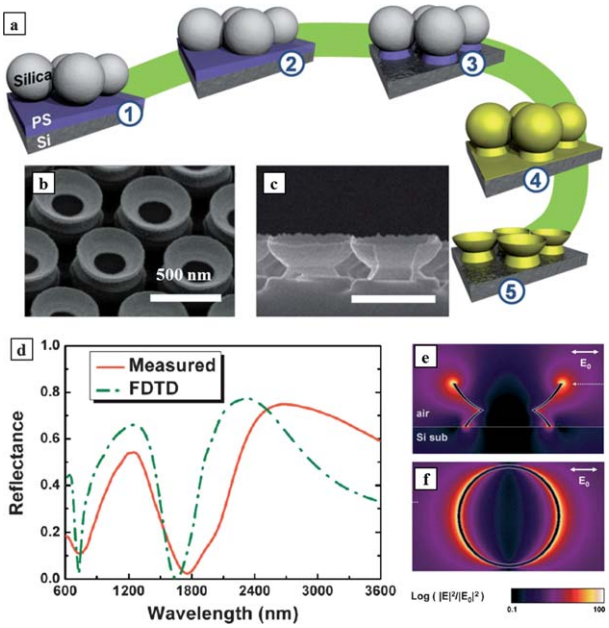

Fig. 3 (a) Schematic representation of the gold nanograil fabrication. (b, c) SEM images of the gold nanograil arrays with tilted view and cross-sectional view, respectively. Scale bars in (b, c) are 500 nm. (d) Comparison of the measured reflectance spectrum with that calculated using the FDTD method. (e, f) Calculated electric field intensity ($|E|^2$) distributions of the plasmon resonances around the nanograil. Reprinted with permission from ref. 23. Copyright 2009 Wiley-VCH Verlag GmbH & Co.

parameters identical to those used in the experiment. The FDTD results, shown in Fig. 3d, also revealed two dips, which agreed well with the measured reflectance data. Normalizing $|E|^2$ by the incident wave intensity $|E_0|^2$ yielded an intensity EF, $\eta = |E|^2/|E_0|^2$ (Fig. 3e and f). The LSPR at 1700 nm displayed a maximum intensity enhancement of $10^{2.2}$ near the top brim of the gold grails. The LSPR at the shorter wavelengths was attributed to the middle ring of the gold grail showing a maximum intensity enhancement of $10^{2.5}$.

2.2 Soft lithography

Simple, robust, and cost-effective soft lithography techniques have been used to fabricate microstructures and nanostructures over large areas. Soft lithography refers to a group of microfabrication techniques that use a mold to pattern a desired material, such as a structured elastomer, in the form of a stamp or conformable photomask.[68,69] The most commonly used elastomer, PDMS, has a low modulus, which can be problematic for pattern transfer and can restrict the utility of this elastomer for patterning in the nanometre regime.[70,71] Improved siloxane-based elastomers display larger moduli, for example, hard PDMS (h-PDMS)[71] or photocurable PDMS (hυ-PDMS),[72] and these materials can extended the resolution of soft lithography to the nanometre region. Composite stamps consisting of a thin layer of structured h-PDMS supported by a soft, thicker layer of soft PDMS (s-PDMS) are usually used for nanoscale patterning due to the difficulties associated with achieving conformal contact using h-PDMS stamps. Soft lithography offers significant advantages over conventional techniques. PDMS molded against a master forms a transparent elastomeric stamp that can be used to fabricate periodic arrays of structures. Moreover, conventional lithographic techniques are required for subsequent processes, such as photolithography, reactive ion etching, wet chemical etching, or electron beam deposition. Finally, one can generate patterns with various shapes, symmetries, and pattern spacing.

In an example of using soft lithography for the fabrication of plasmonic nanostructures, Odom *et al.* developed a SIL technique using nanoscale patterns, made by IL, as soft lithography masters.[73–78] Unlike conventional nanofabrication techniques, SIL can produce plasmonic nanostructures and metamaterials with subwavelength features over large areas.[75,76] Fig. 4a shows a master patterned with arrays of silicon pillars (diameter = 100 nm, height = 400 nm, pitch = 400 nm). A SIL photomask can be replicated from one master pattern by replica molding using a transparent PDMS elastomer. To produce arrays of photoresist posts, a SIL photomask was placed in conformal contact with a positive-tone photoresist on a Si substrate followed by exposure to UV light (Fig. 4b). A second exposure through a chromium (Cr) mask was performed to create microscale patterns of the photoresist posts. A thin Cr layer was deposited by e-beam evaporation followed by lift-off of the photoresist. The exposed Si was anisotropically etched using a KOH/isopropyl alcohol (IPA) solution to form pyramidal voids through Cr nanoholes. A Au layer was then deposited by e-beam evaporation to produce a perforated Au film over the pyramidal Au particles. The sizes of the nanoholes in the arrays were easily controlled by adjusting the etching time. The material and chemical functionalities of these nanostructures could be manipulated *via* deposition of different metals using e-beam evaporation. Finally, Au infinite and finite nanohole arrays were produced over a large area, as shown in Fig. 4c and d. The optical properties of both infinite and finite nanohole arrays were characterized by illuminating the Au films under normal incidence with a white light and collecting the transmitted light in a spectrometer. Fig. 4e and f compare the zero-order transmission spectra of infinite and finite nanohole arrays. The intensities of the plasmon resonances around 500 nm were similar for all spectra. The infinite Au nanohole arrays exhibited peaks corresponding to the Bloch wave SPPs (BW-SPPs) at the Au–glass interface of $\lambda(1,0) = 690$ nm and $\lambda(1,1) = 588$ nm, where (1,0) and (1,1) indicate integer pairs at the Au–glass interface (Fig. 4e). The minimum transmittance of the infinite nanohole array at 660 nm was associated with a Wood's anomaly (WA). In contrast, the spectra of the finite Au nanohole arrays exhibited a lower intensity (1,0) BW-SPP resonance, indicating a decrease in the short-range coupling between nanoholes, and the width of this peak was narrower than that of the infinite array (Fig. 4f).

As with soft lithography, a simple and low-cost soft nanoimprint lithography protocol may be used to generate subwavelength hole arrays over large areas. A topographically patterned PDMS or composite stamp with square arrays of pillars was employed to emboss a thin UV-curable polyurethane film coated onto a glass substrate. The PDMS stamp was pressed into a polyurethane film and exposed to UV light to cure the polyurethane layer. The PDMS stamp was carefully removed, leaving behind a relief structure that corresponded to the pattern on the PDMS stamp. A metal film could then be deposited on the resulting replica structures to fabricate plasmonic nanostructures for chemical and biosensing applications. This emerging technology was employed to replicate patterns on a PDMS or composite stamp on a UV-curable polymeric material or on other low-surface-energy materials. Recently, the research groups of Rogers and Nuzzo fabricated and characterized full and quasi 3D plasmonic crystals using soft nanoimprint lithography.[10,13,79–82] A schematic illustration of soft nanoimprint lithography and an optical photograph of the quasi 3D plasmonic crystals are shown in Fig. 5a and b.[80,82] In this process, an array of posts from a composite stamp, with post diameters of 456 nm, a periodicity of 748 nm, and depths of 350 nm, was used to create cylindrical depression patterns by soft imprint lithography. An optical photograph and SEM image of an embossed plasmonic crystal is shown in Fig. 5b and c.[13] The high-resolution SEM image demonstrates the formation of a continuous gold layer on embossed polyurethane nanowells. Theoretical and experimental transmission spectra of a full 3D plasmonic crystal are shown in Fig. 5d. The features in the transmission spectra of the full 3D plasmonic crystals can be related to LSPRs, WAs, and BW-SPPs, or a combination of these, leading to complex transmission spectra that are sensitive to the structural parameters and the surrounding materials. The normal-incidence transmission spectrum of full 3D plasmonic crystals can be investigated by 3D FDTD calculations. Fig. 5e shows the experimental and theoretical transmission spectra of a 3D crystal in water. It should be noted that the plasmonic features associated with the water–metal interface were red-shifted relative to

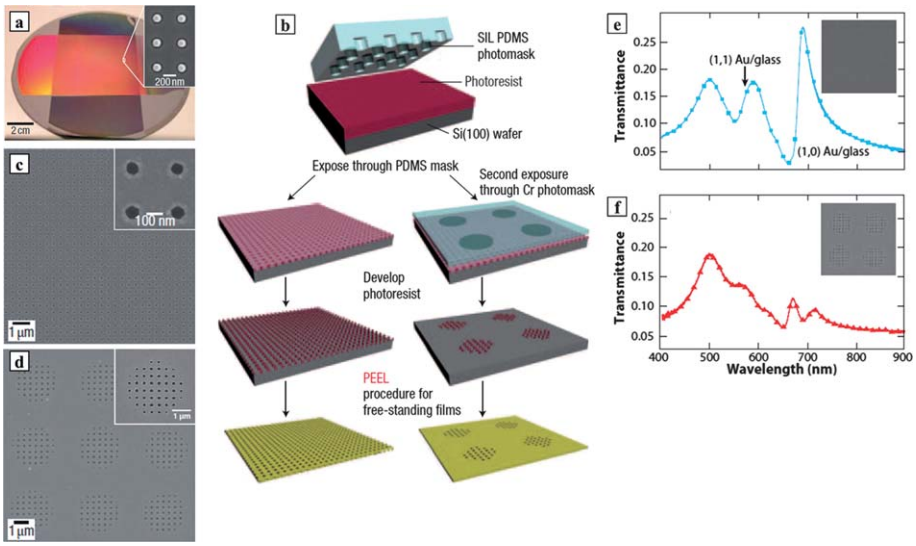

Fig. 4 (a) Optical micrograph of Si master fabricated by interference lithography. Inset shows an SEM image of Si post arrays. (b) Schematic depicting the fabrication process of Au infinite and finite nanohole arrays. (c, d) SEM image of resulting Au infinite and finite nanohole arrays, respectively. Insets in (c and d) show magnified SEM image of infinite and finite nanohole arrays, respectively. Reprinted with permission from ref. 76. Copyright 2007 Nature Publishing. (e) Zero-order transmission spectra of infinite Au nanohole arrays. The Bloch modes are labeled (1,0) and (1,1) and correspond to the (i, j) integer pairs at Au-glass interface. (f) Zero-order transmission spectra of Au finite nanohole arrays. Adapted with permission from ref. 75. Copyright 2009 Annual Reviews.

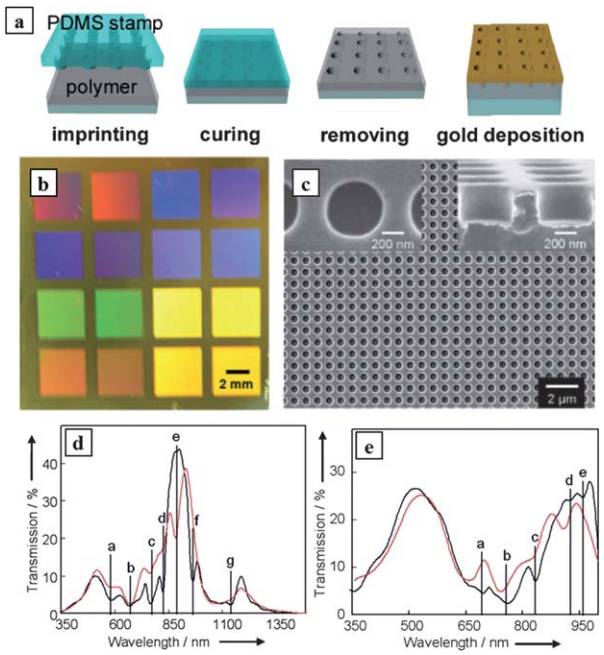

Fig. 5 (a) Schematic illustration of plasmonic crystal fabrication process: imprinting, curing, removing, and gold deposition. (b) Optical photograph of an embossed plasmonic crystal. (c) SEM image of a 3D plasmonic crystal. Left inset is a top view of SEM image. Right inset is a high-magnification SEM that shows the continuous gold layer on the embossed nanowell arrays. Reprinted with permission from ref. 82. Copyright 2010 Wiley-VCH Verlag GmbH & Co. KGaA. (d) Transmission spectrum of a 3D plasmonic crystal in air (red) and theoretical transmission spectrum of a 3D plasmonic crystal by 3D FDTD calculations (black). (e) Experimental and theoretical transmission spectra of a 3D plasmonic crystal in water. Adapted with permission from ref. 13 Copyright 2008 Wiley-VCH Verlag GmbH & Co. KGaA.

those for the air–metal interface because the surrounding dielectric constant was higher. Three-dimensional FDTD calculations showed that the sensitivity of these features increased as the nanohole diameter increased and the nanohole spacing decreased.

2.3. Template-based methods

The nano/micro porous membranes that have been successfully fabricated using various techniques provide excellent platforms on substrates, deposition or etching masks, or substrates for fabricating periodic submicron-sized diverse metal structures exhibiting plasmonic properties.

Here, three representative techniques used to fabricate templates for generating a variety of plasmonic nanostructures are discussed: IL,[48,83–89] BCP,[90–93] and porous alumina templates.[94–98] These techniques are usually facile, cost-effective, and manufacturable over large areas.

Interference lithography, which is a maskless lithography technique based on the interference of multiple coherent light beams, has been employed to fabricate submicron scale defect-free periodic structures using photoresists. The precise control over the gap separation and shape of the nanostructures is enabled by changing the fabrication conditions during IL, such as the laser exposure dose,[85,88,89] the angles and phases between the adjacent beams,[86–89] and the polarization of the light.[83,89] Therefore, IL can be used to fabricate a variety of large-area patterned metallic nanoscale structures that display plasmonic properties. Lithographically defined polymeric nanopatterns may be used as masks for the deposition of metal thin films.[48,83,84,87,89] The tunable vacant hole and pitch of the polymeric masks ultimately determine the plasmonic nanostructures after the deposition step. Removal of the photoresist can be

accomplished without impacting the uniformly arranged metal nanostructures.[48,83,84,87,89]

A variety of well-defined plasmonic nanostructures developed from IL are shown in Fig. 6. Liu *et al.* used laser IL to fabricate polymeric 2D nanostructures for patterning bimetallic (Au–Ag) dot structures that yielded an SPR band that was blue-shifted compared to the plasmon band arising from single Au dot arrays (Fig. 6a).[84] Furthermore, multi-layered metallic metamaterials can be formed using IL. A series of pairs of elliptical metal (Ag)–dielectric (SiO_2)–metal (Ag) plates (PEMDMPs) with a range of major and minor axis lengths was fabricated by Li *et al.* (Fig. 6b and c).[87] The geometrical features of the elliptical nanostructures could be altered by varying the angles of the laser beams. The magnetic 1D (Fig. 6d) and 2D metamaterials (Fig. 6e) with magnetic dipole resonances at 1.2 μm were fabricated over large areas *via* compact multi-beam IL using suitably shaped dielectric roof-top prisms or pyramids.[83] As shown in Fig. 6f, the large-area plasmonic substrates consisted of Au nanoholes patterned in a regular microarray of 200 μm diameter circular patches that could be used for SPR imaging and, potentially, in multiplex biosensing applications, were fabricated using both interference and conventional optical lithography.[48] Twin and triplet motif features with plasmonic nanogaps 70 times smaller than the laser wavelength have recently been achieved (Fig. 6g).[89] The relative spacings of the sublattices could be tuned by controlling the phase, polarization, and laser beam intensity during 4-beam IL. In addition, Li *et al.* used IL-featured structures as templates for fabricating 2D metallic arrays with different hole sizes (Fig. 6h and i),[85] aspect ratios, and periods (Fig. 6j and k)[86] to investigate the effects on the SPPs. Using a similar approach, cylindrical metal nanocluster arrays composed of Au NPs 835 nm in pitch and 415 nm in diameter were fabricated by Lee *et al.* (Fig. 6l).[88]

Two or more covalently bonded homopolymers can form a BCP. Self-assembled BCPs that yield spherical, cylindrical, and lamella morphologies are emerging as scaffolds or templates for the fabrication of nanostructured materials over large surface areas on the sub-100 nm scale.[27,90–93] The dimensions of the domains can be easily tuned by changing the total molecular weight of the BCP.[90,91] The morphology of a self-assembled BCP can provide a platform for producing highly ordered metallic nanostructures, as shown in Fig. 7. Lu *et al.* fabricated Ag surfaces with periodically ordered nanoscale features that were capable of producing enhanced Raman signals using a self-organized inorganic BCP template (Fig. 7a).[90] The size and spacing of the nanostructures could be adjusted by tailoring the polymer chain length. Fig. 7b shows dense ordered large-area arrays of Au NPs on various substrates, demonstrating the variability of the SPPs. These arrays were produced by reducing metal salts on the BCP templates formed by solvent annealing of a BCP thin film in a mixed solvent.[92] Wang *et al.* fabricated dense arrays of mushroom-shaped Au nanopillars with a period of 50 nm over a large area using simple BCP-templated galvanic displacement reactions to produce coupling among adjacent mushroom caps. These structures produced a high spatial density

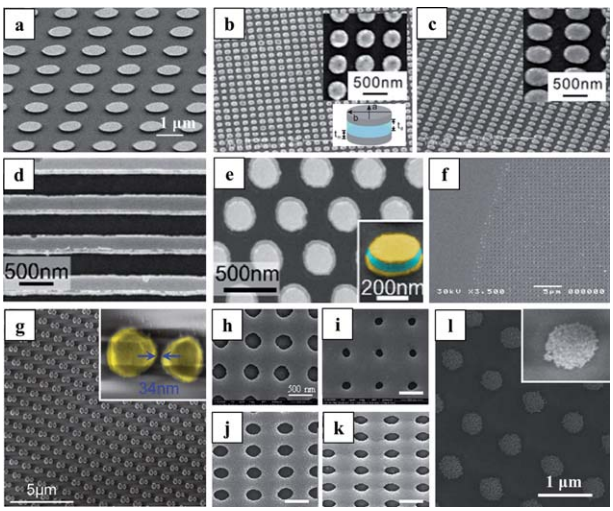

Fig. 6 SEM images of a variety of metallic nanostructures using IL. (a) 2D bimetallic (Au–Ag) dot arrays. Reprinted with permission from ref. 84. Copyright 2008 Optical Society of America. PEMDMPs with a fixed minor axis of 350 nm but a varied major axis of (b) 350 nm and (c) 504 nm, respectively. Reproduced with permission from ref. 87. Copyright 2010 Optical Society of America. (d) 1D and (e) hexagonal 2D metamaterials. Reprinted with permission from ref. 83. Copyright 2007 Optical Society of America. (f) Periodic arrays of nanoholes in one of the circles of the microarray. Reprinted with permission from ref. 48. Copyright 2010 Wiley-VCH Verlag GmbH & Co. KGaA. (g) The bowtie shaped pattern arrays. Reproduced with permission from ref. 89. Copyright 2011 American Chemical Society. Metallic hole arrays with different hole radii of (h) 177 nm and (i) 87 nm. Reproduced with permission from ref. 85. Copyright 2009 American Institute of Physics. Elliptical metallic hole arrays with different aspect ratios with (j) 1.35 and (k) 1.67. Reproduced with permission from ref. 86. Copyright 2009 American Institute of Physics. (l) Cylindrical Au nanocluster arrays. Reproduced with permission from ref. 88. Copyright 2009 Optical Society of America.

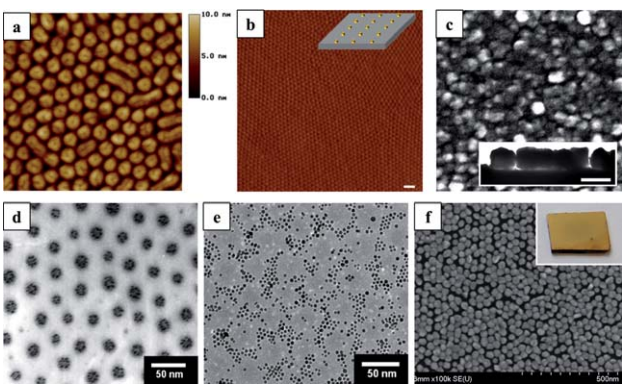

Fig. 7 (a) AFM height image of an array of inorganic cylinders. Reprinted with permission from ref. 90. Copyright 2006 Institute of Physics. (b) Au nanoparticle arrays after removing the BCP template. Reprinted with permission from ref. 92. Copyright 2009 American Chemical Society. (c) SEM images of nanostructured Au film obtained by plating for 90 s. The inset shows a TEM image of cross-sectional specimen. Reproduced with permission from ref. 93. Copyright 2009 American Chemical Society. (d, e) TEM images of metal-BCP composite films with different composition of micelles. Reprinted with permission from ref. 91. Copyright 2009 American Chemical Society. (f) SEM image of Au nanoparticle arrays on the quaternized BCP film. The inset shows photograph of Au nanostructures. Reproduced with permission from ref. 27. Copyright 2011 Wiley-VCH Verlag GmbH & Co. KGaA.

of hot spots in the narrow gaps (Fig. 7c).[93] Novel methods for fabricating thin films of self-assembled metal–BCP composite micelles based on spin coating have been described by Acharya *et al.* (Fig. 7d and e).[91] These films, which displayed SP bands, were formed by the position-selective deposition of Au and Ag NPs. Fig. 7f shows that self-assembled Au nanospheres provided extended SPR tuning over the range 520–1000 nm *via* control over the nanosphere diameter and spacing, guided by a chemically modified BCP template.[27]

An effective method for fabricating ordered arrays involves self-organized nanoporous templates of anodized aluminum oxide (AAO). This approach has attracted attention as a direct route to fabricating metallic nanoarrays due to its many advantages, such as long-range ordering, mechanical stability, and facile controllability of the shape configurations by varying the conditions of the anodization process.[94–98] Fig. 8 shows images of ordered metallic nanorod arrays formed on porous AAO templates. Shaban *et al.* fabricated vertically aligned free-standing Au nanorods with tunable aspect ratios using DC electrodeposition onto a modified porous AAO template in an alumina etching solution (Fig. 8a).[97] The strong SPR shown in the fabricated nanostructures could be tuned by changing the aspect ratio and dielectric environment. As shown in Fig. 8b, Au–polymer nanocomposite plasmonic nanorod arrays in AAO templates exhibited a complex response in the visible and near-infrared (NIR) and could be fabricated from Au NPs in conjunction with the polymerization of a photosensitive polymer.[96] Choi *et al.* fabricated nonlithographic composite nanoplasmonic substrates by controlling the thicknesses of the metal and AAO to investigate the effects on the EM field enhancements for sensing applications (Fig. 8c).[94] Arrays of Ag NPs[98] and Ag–silica hybrid nanowires[95] with precisely tunable sub-100 nm coupling gap distances, which enhanced the Raman signal intensity for molecular detection, are shown in Fig. 8d and e, respectively.

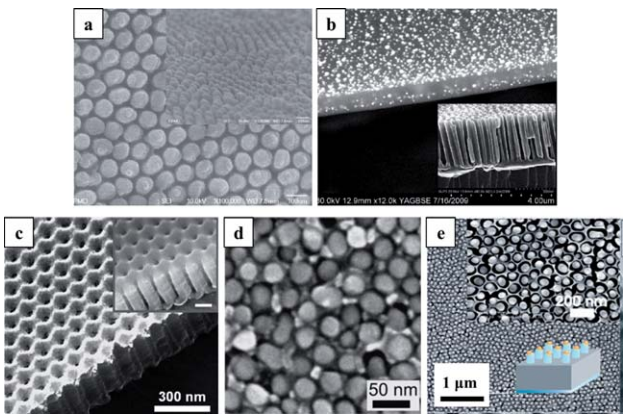

Fig. 8 SEM images of various metallic nanostructure arrays. (a) The free-standing Au nanorod arrays after deposition and removing steps. Reprinted with permission from ref. 97. Copyright 2010 American Scientific Publishers. (b) Au-polymer composite plasmonic arrays in AAO template (Inset: bare AAO template). Reprinted with permission from ref. 96. Copyright 2010 American Chemical Society. (c) The Au-evaporated nanopore arrays. The insets shows the AAO template before Au evaporation (scale bar: 100 nm). Reprinted with permission from ref. 94. Copyright 2010 Wiley-VCH Verlag GmbH & Co. KGaA. (d) The grown Ag nanoparticles in the AAO substrate. Reprinted with permission from ref. 98. Copyright 2006, Wiley-VCH Verlag GmbH & Co. KGaA. (e) The individual silica rod arrays with encapsulated Ag nanoparticle. Reprinted with permission from ref. 95. Copyright 2006 Wiley-VCH Verlag GmbH & Co. KGaA.

3. Applications of plasmonic nanostructures

3.1. Optical sensing based on changes in refractive index

As mentioned in the introduction, SPs strongly depend on the type, size, shape, and surrounding dielectric environment of the nanostructures.[99] A strong peak or dip at a specific wavelength in the optical spectrum can be tuned over the visible and NIR ranges by changing the aforementioned factors. Sensitivity to changes in the RI of the local environment around metallic nanostructures, which can tune the optical properties of the nanostructures, has remarkable potential in optical sensing.[23,48,76,100–102] Unlike conventional optical sensor applications, SP-based sensors have a high sensitivity for the label-free detection of surface binding events; hence, several plasmon-based sensors have been developed for monitoring the binding of biological or chemical analytes on suitable metallic surface structures in real-time by measuring the SPR signal enhancement and shifts. To this end, several fabrication methods have been used to develop plasmon-based sensing platforms.

Fig. 9 shows several metallic nanostructures designed for optical sensing of local RI changes. Fig. 9a shows the measured reflectance spectra obtained from Au nanograils using various solvents with RI values between 1.33 and 1.50.[23] The position of the optical dip shifted toward longer wavelengths as the RI increased. A higher LSPR sensitivity could be achieved by varying the top and middle diameters of the Au nanograils. The binding of analyte molecules to the ligand-modified nanoparticles shifted the plasmon band relative to that of the nanopattern prior to binding kinetic measurements.[101] These properties are widely employed in biomolecular sensing applications. Van Duyne and co-workers prepared an array of Ag nanotriangles for use in nanobiosensing applications based on LSPR. The Ag nanotriangles were prepared from a nanosphere deposition mask.[101] Fig. 9b shows the LSPR shift resulting from interactions between the amyloid β-derived diffusible ligands (ADDL) and an anti-ADDL antibody as a function of the concentration of anti-ADDL antibody, which may be relevant to the development of Alzheimer's disease.[101] Kubo and Fujikawa fabricated Au double nanopillar arrays with nanogaps on the order of several tens of nanometres, constructed by alternately laminating thin layers of Au and polymer on a template *via* nanoimprinting and layer-by-layer (LBL) techniques (Fig. 9c).[100] The Au double nanopillar arrays with 33 nm gaps showed red-shifted plasmon resonance peaks in proportion to the RI variations and exhibited a high RI sensitivity of 1075 nm/RIU, which can improve sensor performance (Fig. 9d).[100] The metal nanostructure sensitivity was characterized by a higher sensor figure of merit than the alternative structures that did not have nanogaps but had almost equivalent surface areas. Fig. 9e illustrates the tunability of the optical properties of the infinite Au nanohole arrays on glass, which could be fabricated *via* high-throughput soft IL by changing the RI of the top surface using

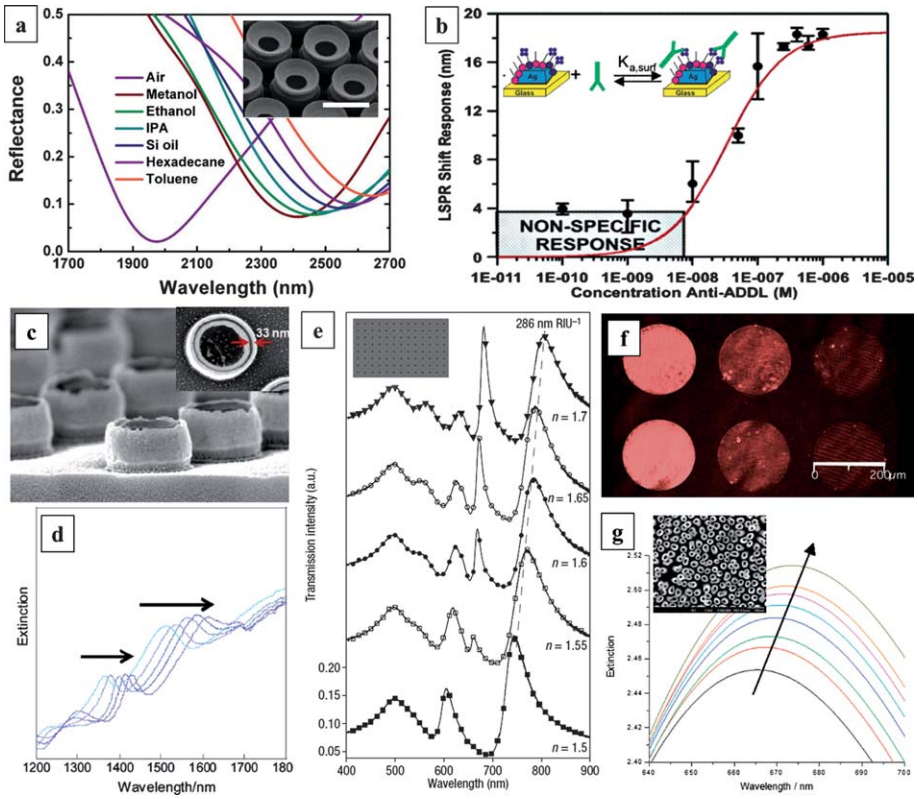

Fig. 9 (a) Measured reflectance spectra of Au-nanograils in response to solvent media with different refractive indices. Reproduced with permission from ref. 23. Copyright 2009 Wiley-VCH Verlag GmbH & Co. KGaA. (b) LSPR shift, $\Delta\lambda_{max}$ *versus* [anti-ADDL antibody] response curve for the binding of anti-ADDL antibody to an ADDL-functionalized Ag nanobiosensor. The inset shows design of the LSPR biosensor for anti-ADDL detection. Reproduced with permission from ref. 101. Copyright 2004 American Chemical Society. (c) SEM images of Au double nanopillar arrays with nanogap width of 33 nm, and (d) their extinction spectra under various refractive indices. Reproduced with permission from ref. 100. Copyright 2011 American Chemical Society. (e) Zero-order transmission of infinite Au hole arrays in the variuos immersion liquids. Reprinted with permission from ref. 76. Copyright 2007 Nature Publishing Group. (f) SPR Image from a microarray of periodic arrays of nanoholes integrated in a microfluidics device in air, water, and glucose solution (from left to right). Reproduced with permission from ref. 48. Copyright 2010 Wiley-VCH Verlag GmbH & Co. KGaA. (g) Extinction spectra for different concentrations of glycerol in water acquired for both inside and outside walls exposed. The inset shows the SEM image of the Au nanotube arrays. Reproduced with permission from ref. 102. Copyright 2010 American Chemical Society.

different RI immersion liquids.[76] The SPP peaks for the infinite Au nanohole arrays became red-shifted as the RI of the surrounding environment increased, but the bulk plasmons remained unchanged. This group also measured the plasmonic spectra of the arrays made of metal (Au) or a dielectric material (Si). The Au nanohole arrays were integrated into three-channel microfluidic devices fabricated through a combination of conventional optical lithography. The arrays displayed different SPR spectra when contacted with different dielectric media, and the intensity of the transmitted light varied with the RI of the medium in contact with the Au hole arrays (Fig. 9f).[48] The detection of adsorption events in which streptavidin bound to the gold nanostructured surfaces was tested with the goal of preparing an SPR bioaffinity biosensor. McPhillips *et al.* fabricated Au nanotube arrays that supported plasmonic resonances by electro-deposition of Au around the polypyrrole nanorods in a thin AAO template.[102] Fig. 9g suggests that Au nanotubes may potentially act as high-performance RI sensors of biomolecular binding reactions, provided that the detection conditions could be optimized. Exposure of both the inside and outside walls increased the red-shift of the extinction peaks, corresponding to an increase in the RI, and the intensity of the extinction also increased. This behavior is not entirely understood because exposure of the inner nanotube walls increased the RI, which resulted in a red shift; however, the extinction peak decreased.

3.2. Surface enhanced Raman scattering (SERS)

Raman scattering inelastically happen when light interacts with matter of the analyte molecule. Then, incident photons may gain energy from, or lose it to the vibrational or rotational excitations.[103] The Raman effect represents a concomitant shift in the frequency of the scattered light caused by a change in the photon energy. The Raman spectra include specific bands that provide information about the molecular structure and composition of the analyte, similar to a chemical fingerprint. However, the intensity of the Raman spectra is very weak. Typical Raman cross-sections range from 10^{-31} to 10^{-25} cm^2/molecule.[104]

In the 1970s, Fleischmann and co-workers reported a dramatic increase in the Raman signal intensity from molecules adsorbed onto roughened noble metal surfaces due to EM field enhancements on the surface.[105] Since then, efforts have been applied

toward enhancing the intensity of the Raman signals, which depend on the type, size, roughness, and shape of the metal NPs, excitation wavelength, and intensity of the incident light field.[103,104] This phenomenon, called surface enhanced Raman scattering (SERS), presents a powerful strategy for detecting numerous chemical and biological molecules. SERS-based detection has several advantages over fluorescence detection, including rapid label-free identification of analytes, Raman spectral linewidths are 10–100 times narrower than fluorescence labels, and label time-dependent photobleaching is not an issue. If the excitation laser wavelength is well-matched to the LSPR absorption band of the metallic nanostructure substrates, a stronger SERS signal can be achieved.[27]

A variety of techniques have been developed for fabricating roughened metallic nanostructures as SERS substrates with optimal geometric features for sensing applications. Fig. 10 shows a variety of metal nanostructures for SERS applications. The simplest approach to their fabrication is CL.[26,29–31] A monolayer of colloidal particles is prepared to form a mask for metal deposition or a template for nanopatterning a metal thin film. The colloidal particle masks can then simply be removed. According to this technique, the size and period of the resulting metallic structures can be easily adjusted by varying the size of the colloidal particles. Fig. 10a shows colloidal lithographically fabricated 300 nm thick Ag nanobowl arrays,[30] which are hierarchical structures composed of Ag NPs with an average diameter of 10 nm, using thermal evaporation and sticking tape. A very strong SERS signal was obtained using p-nitroaniline as a probe molecule upon excitation of the metal SP and confinement of the probe in the high EM field of the Ag cavity. This signal was much higher than that obtained from a reference Ag film. Yang *et al.* fabricated surface nanopatterned nanoshell arrays with well-defined structures using electrophoresis of Ag colloidal solutions on polystyrene (PS) sphere templates

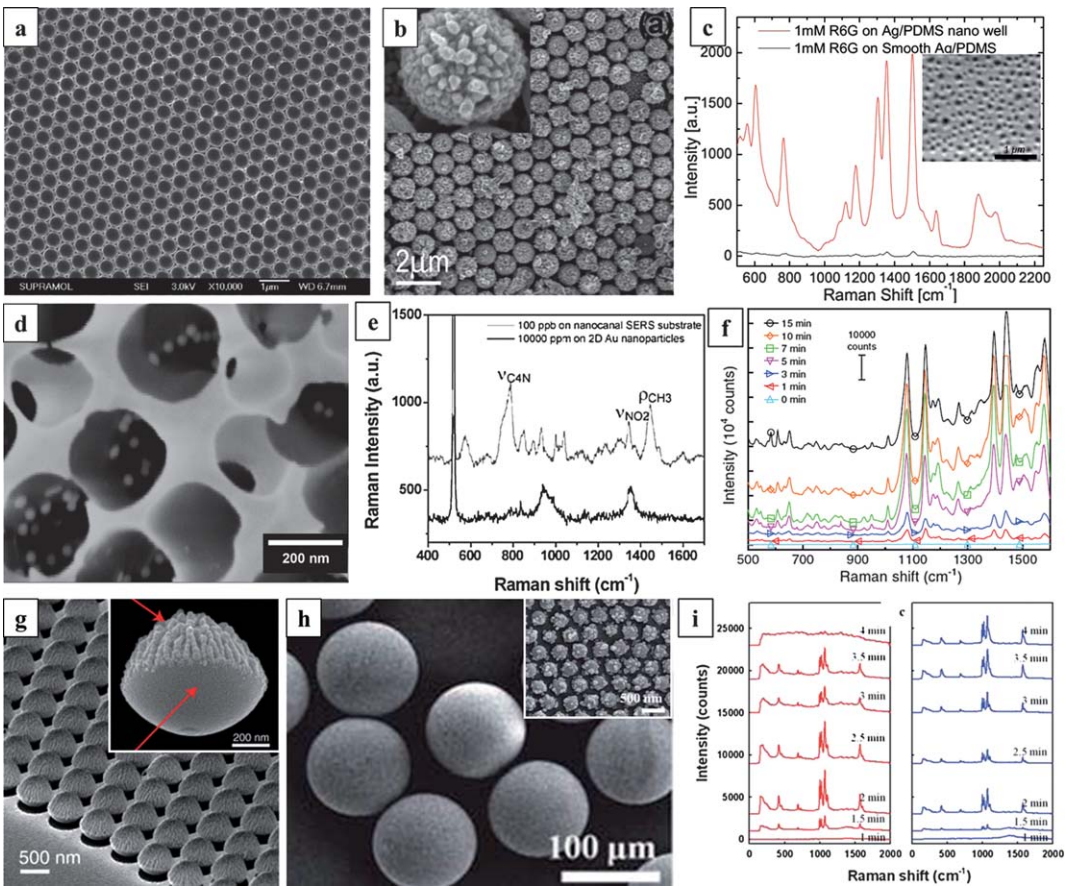

Fig. 10 SEM images and Raman spectra of various metallic nanopatterned structures as SERS substrates. (a) Ag nanobowl arrays on the tape. Reprinted with permission from ref. 30. Copyright 2009 American Chemical Society. (b) Ag nanoshell arrays covered PS nanospheres. Reprinted with permission from ref. 31. Copyright 2010, Wiley-VCH Verlag GmbH & Co. KGaA. (c) SERS spectra of R6G molecules in a microfluidic channel taken from the Ag/PDMS nanowell substrate (upper) and the smooth Ag/PDMS substrate (lower). The inset shows Ag nanowells on a PDMS chip. Reproduced with permission from ref. 28. Copyright 2005 American Institute of Physics. (d) Au decorated porous alumina membrane and (e) their Raman spectra of 2,4-dinitrotoluene comparing with 2D substrate. Reproduced with permission from ref. 107. Copyright 2008 Wiley-VCH Verlag GmbH & Co. KGaA. (f) SERS spectra of 4-aminobenzenethiol on the series of Au nanoparticle arrays on the quaternized BCP film. Reprinted with permission from ref. 27. Copyright 2011, Wiley-VCH Verlag GmbH & Co. KGaA. (g) Nanocoral arrays (inset: free-floating nanocoral probe). Reproduced with permission from ref. 29. Copyright 2010, Wiley-VCH Verlag GmbH & Co. KGaA. (h) Monodisperse microspheres anchoring Ag-decorated silica nanoparticles and (i) their SERS spectra of benzenethiol prepared using various silver deposition times, measured from microspheres in air (red) and ethanol (blue). Reproduced with permission from ref. 26. Copyright 2011 The Royal Society of Chemistry.

(Fig. 10b).[31] The SERS properties, which yielded a high EF on the order of 10^7, could be easily controlled by adjusting the structural parameters (the diameter, intershell spacing, and surface roughness) of the nanoshells by varying the electrophoretic deposition and plasma etching times. Lee's group fabricated SERS substrates in microfluidic biochips for label-free detection of biochemical reactions in multiplexed aqueous environments. The Ag/PDMS nanowell structures,[28] which create SERS active sites, were created by soft lithography and selective deposition of Ag. Using a 785 nm laser, they demonstrated the ultra-sensitivity of these nanostructures as SERS substrates. The Raman signals of target molecules adsorbed onto nanowell structures were a factor of 10^7 higher than the Raman signals obtained from smooth Ag layer on PDMS (Fig. 10c).

Another approach to increasing the sensitivity of SERS has involved developing 3D porous structures as potential SERS substrate templates due to the large surface area of such structures, which can form a higher concentration of hot spots for target molecule absorption.[106–108] Fig. 10d shows nanocanal arrays composed of uniformly aligned vertical pores with the inner walls decorated with Au NPs.[107] Porous alumina membranes with modified surfaces were decorated with Au NPs. The Raman peak intensities of the 3D nanocanal substrates were higher than those of the 2D substrates (Fig. 10e). The detection limit of target analyte adsorption onto the nanocanals could be as low as 10 fg. This limit was two orders of magnitude better than the best detection results reported previously using NIR laser (785 nm) because transmission through the aluminum membrane was higher.

Lee *et al.* measured the SERS spectra (shown in Fig. 10f) of 4-aminobenzenethiol on a series of substrates modified with arrays of self-assembled Au nanospheres prepared using different overgrowth times, from 1 to 15 min (see Fig. 7f).[27] They demonstrated that a maximal EF with a 10% standard deviation and an SPR red-shifted with respect to the SERS instrument laser line was obtained by tuning the nanosphere diameter and spacings. Nanoparticle-based SERS enhancements have been pursued to circumvent the limitations associated with nanopatterned substrate-based SERS detection, such as the slow binding kinetics owing to limited mobility.[26] Fig. 10g and h show SERS-active particles fabricated using colloidal nanoparticles as templates for metal deposition. Wu *et al.* described the preparation of bioinspired nanocorals that were then used to perform two decoupled functions involving biomolecular sensing and cellular targeting (Fig. 10g).[29] The top surfaces of the nanocorals were highly roughened with Au to create a high density of hot spots for SERS applications, and the PS hemispheres on the bottom surface could be selectively functionalized with antibodies to bind to breast cancer cells. The SERS performance, which provided a maximum SERS EF of 6.5×10^7, could be altered by controlling the fabrication conditions, such as the PS etching time and the thickness of the deposited Au films. Hwang *et al.* fabricated monodisperse microspheres with hierarchical surface nanopatterns using a microfluidic system (Fig. 10h).[26] Silica nanoparticles anchored to the microparticles provided templates for Ag decoration during the electroless deposition process. The hierarchical surface morphologies of the microspheres, which directly affected the SERS activity, could be controlled by varying the Ag deposition time (Fig. 10i). A Ag microparticle deposition time of 2 min yielded an excellent SERS EF value of 9.3×10^6. Nanoparticles-based SERS templates have significant potential for use in real-time label-free sensing applications in microfluidic systems.

3.3. Plasmonic-enhanced photovoltaics

Plasmon-enhanced photovoltaics are an interesting area of research among the plasmonic applications.[40,48,109–111] Photovoltaic cells can be combined with metallic nanostructures that concentrate and manipulate light on the nanoscale, thereby increasing the absorption of incident light. Plasmonic structures permit the thickness of photovoltaic absorption layers to be reduced while retaining a constant optical absorption coefficient. Three light-trapping configurations have been identified for use in thin film photovoltaic cells. First, metal NPs can be used as subwavelength scattering objects to trap sunlight within the semiconductor at the surface of the solar cell (Fig. 11a). Second, metal NPs can be used as subwavelength elements, in which the near-field plasmons are coupled to the semiconductor layer to create electron–hole pairs, thereby increasing the absorption cross-section (Fig. 11b). Third, light may be trapped by excitation of SPPs at the metal–semiconductor interface. A back metal surface can couple light to SPPs or guided modes that propagate in the plane of the semiconductor layer (Fig. 11c).

The enhanced coupling of light into semiconductor thin film requires the integration of metal nanostructures and control over feature dimensions at the nanometre scale. Although lithographic approaches can be used to prepare plasmonic solar cell structures, including FIB milling or EBL, practical large-area photovoltaic cell structure applications require inexpensive and scalable techniques for producing metal nanostructures. Some research groups have explored these techniques and have achieved improved solar cell performances. An easy way to form metal NPs on a substrate is to thermally evaporate a thin metal film (10–20 nm) onto a substrate that is heated to a high temperature (200–300 °C). As shown in Fig. 11d, this process leads to the creation of random arrays of Ag NPs 100–150 nm in diameter and hemispherical shapes that are suitable for light trapping.[47] To achieve precise control over the Ag NP size, density, and aspect ratio, a porous alumina template has been used during deposition (Fig. 11e).[49] Substrate conformal imprint lithography using a sol–gel mask defined by soft lithography was also demonstrated. The subsequent Ag evaporation and lift-off processes led to the formation of hexagonal arrays of Ag NPs over large areas (Fig. 11f).[40]

More recently, Brolo *et al.* demonstrated that periodic arrays of nanoholes (PANHs) in gold films fabricated by IL could be used for plasmon-enhanced photovoltaics.[48] SEM images of top (inset) and cross-sectional views of the photoresist templates on glass substrates are shown in Fig. 11g. The photoresist template is composed of high aspect ratio cylindrical pillars. Fig. 11h shows SEM images of the PANHs in Au films after deposition of a Au film and lift-off of the photoresist template. PANHs, which were used as back electrodes, can couple light to the propagating SP waves to increase the creation of charge carriers. Fig. 11i shows the photocurrent spectra for two photovoltaics, in which the incident photon to current efficiency (IPCE) is plotted as a function of the illumination wavelength. One photovoltaic used

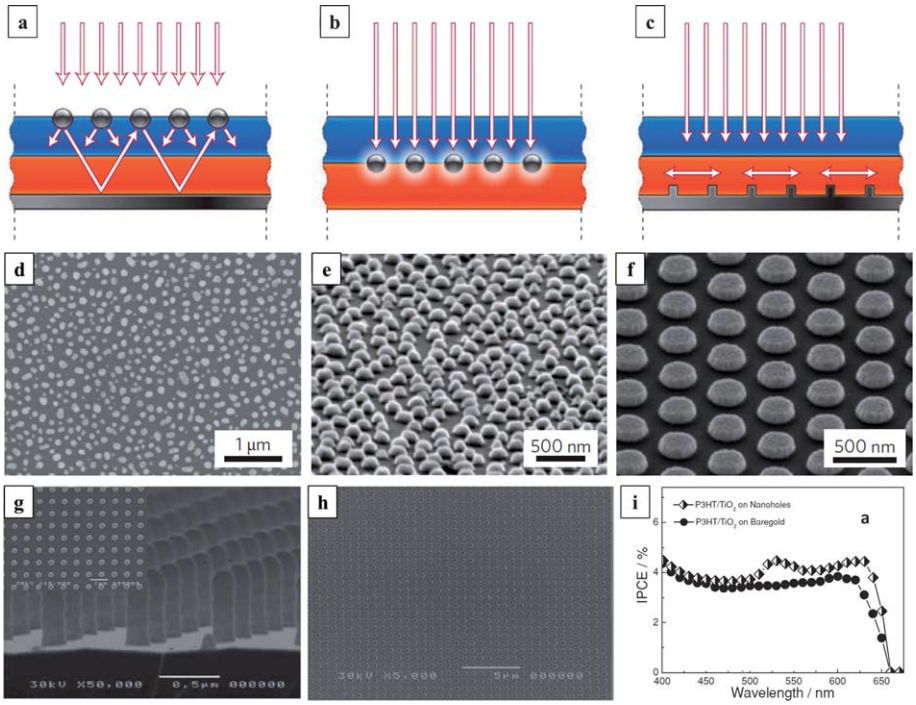

Fig. 11 (a) Light trapping by scattering from metal NPs at the surface of the solar cell. (b) Light trapping by the excitation of LSPR in metal nanoparticles embedded in the semiconductor. (c) Light trapping by the excitation of SPPs at the metal/semiconductor interface. A patterned metal back surface couples light to SPP or guided modes that propagate in the plane of the semiconductor layer. (d) A 14 nm thick Ag film was deposited onto a thermally oxidized Si wafer by thermal evaporation and annealed at 200 °C in a N_2 ambient atmosphere. (e) Silver nanoparticles evaporated through a porous alumina template, annealed at 200 °C. (f) Hexagonal array of Ag nanoparticles deposited using substrate-conformal imprint lithography. Reproduced with permission from ref. 40. Copyright 2007 Nature Publishing. (g) SEM images of photoresist template on glass substrate. Inset show top view of photoresist template. (h) SEM image of the PANHs in Au film after the deposition of Au film and the lift-off of the photoresist template. (i) IPCE plots of P3HT:TiO_2 photvoltaic using a large area PANHs. Adapted with permission from ref. 48. Copyright 2007 Wiley-VCH Verlag GmbH & Co. KGaA.

a smooth gold film as an anode and the other used a large area PANHs as an SPR active anode fabricated by IL. Polymer solar cells with thin layers based on poly-3-hexylthiophene (P3HT) have been prepared. P3HT is a conjugated polymer that significantly improves the performance of polymer photovoltaic cells or solar cells based on nanocomposite films containing P3HT and TiO_2 nanoparticles. The relationship between the IPCE and the wavelength (Fig. 11i) reveals that P3HT/TiO_2 photovoltaics in which large-area PANHs act as SPR-active anodes exhibit a higher photocurrent than that of P3HT/TiO_2 photovoltaics based on bare gold surfaces, over the range of 520–630 nm.

4. Conclusions

Studies and applications of plasmonic nanostructures fabricated by unconventional methods have moved beyond small metal NPs in terms of analytical sensitivity and versatile mode of operation. Plasmonic nanostructures are important functional materials for a variety of promising applications ranging from SP-based photonics to biotechnology. Through new and creative methodologies, a variety of plasmonic materials have been prepared, including 2D or 3D metal nanopatterns and complex plasmonic nanostructures. In this review, we have discussed studies related to unconventional methods for fabricating plasmonic structures, as well as the chemical or biosensing applications of nanostructured plasmonic materials. The methods developed in these studies can overcome several limitations on the fabrication of plasmonic structures, such as restrictions on feature shape, feature size, and total area over which plasmonic structures are patterned. The LSPR-active plasmonic nanostructures described here display outstanding performances and are prepared using versatile and reproducible methods. These studies demonstrate the effect of nanostructure shape, size, aspect ratio, and material composition on both the LSPR spectral features and the spectral sensitivity to changes in the local dielectric environment.

Metallic nanostructure design optimization and recent advances in LSPR sensing using plasmonic structures represent significant progress toward high-sensitivity LSPR biosensors; however, the plasmonic materials developed thus far do not yet meet the requirements for material robustness and consistency. The practical utility of LSPR biosensors in the analysis of complex solutions requires biosensors to be capable of detecting multiple analytes in very small sample volumes. The most versatile and promising approaches involve microfluidic systems, which show promise as commercial LSPR platforms. Theoretical studies have provided practical guidance toward optimizing the spectroscopic performance. Future studies should seek to further develop effective and exact theoretical approaches to optimizing these systems.

Acknowledgements

This work was supported by a grant from the Creative Research Initiative Program of the Ministry of Education, Science and Technology for "Complementary Hybridization of Optical and Fluidic Devices for Integrated Optofluidic Systems." The authors also appreciate partial support from the Brain Korea 21 Program.

Notes and references

1 W. L. Barnes, A. Dereux and T. W. Ebbesen, *Nature*, 2003, **424**, 824.
2 S. Lal, S. Link and N. J. Halas, *Nat. Photonics*, 2007, **1**, 641.
3 J. H. Fendler and E. Hutter, *Adv. Mater.*, 2004, **16**, 1685.
4 J. Zhao, X. Y. Zhang, C. R. Yonzon, A. J. Haes and R. P. Van Duyne, *Nanomedicine*, 2006, **1**, 219.
5 E. C. Nice and B. Catimel, *BioEssays*, 1999, **21**, 339.
6 J. Homola, *Anal. Bioanal. Chem.*, 2003, **377**, 528.
7 N. Nath and A. Chilkoti, *Anal. Chem.*, 2004, **76**, 5370.
8 T. W. Ebbesen, H. J. Lezec, H. F. Ghaemi, T. Thio and P. A. Wolff, *Nature*, 1998, **391**, 667.
9 L. J. Sherry, S. H. Chang, G. C. Schatz, R. P. Van Duyne, B. J. Wiley and Y. N. Xia, *Nano Lett.*, 2005, **5**, 2034.
10 M. E. Stewart, N. H. Mack, V. Malyarchuk, J. A. N. T. Soares, T. W. Lee, S. K. Gray, R. G. Nuzzo and J. A. Rogers, *Proc. Natl. Acad. Sci. U. S. A.*, 2006, **103**, 17143.
11 C. R. Yonzon, E. Jeoungf, S. L. Zou, G. C. Schatz, M. Mrksich and R. P. Van Duyne, *J. Am. Chem. Soc.*, 2004, **126**, 12669.
12 J. N. Anker, W. P. Hall, O. Lyandres, N. C. Shah, J. Zhao and R. P. Van Duyne, *Nat. Mater.*, 2008, **7**, 442.
13 J. M. Yao, M. E. Stewart, J. Maria, T. W. Lee, S. K. Gray, J. A. Rogers and R. G. Nuzzo, *Angew. Chem., Int. Ed.*, 2008, **47**, 5013.
14 A. G. Brolo, E. Arctander, R. Gordon, B. Leathem and K. L. Kavanagh, *Nano Lett.*, 2004, **4**, 2015.
15 A. G. Brolo, A. De Leebeeck, L. K. S. Kumar, V. de Lange, D. Sinton and R. Gordon, *Anal. Chem.*, 2007, **79**, 4094.
16 E. M. Hicks, S. L. Zou, G. C. Schatz, K. G. Spears, L. Gunnarsson, T. Rindzevicius, B. Kasemo, M. Kall and R. P. Van Duyne, *Nano Lett.*, 2005, **5**, 1065.
17 Q. M. Yu, P. Guan, D. Qin, G. Golden and P. M. Wallace, *Nano Lett.*, 2008, **8**, 1923.
18 S. A. Maier, P. G. Kik, H. A. Atwater, S. Meltzer, E. Harel, B. E. Koel and A. A. G. Requicha, *Nat. Mater.*, 2003, **2**, 229.
19 A. N. Grigorenko, N. W. Roberts, M. R. Dickinson and Y. Zhang, *Nat. Photonics*, 2008, **2**, 365.
20 E. M. Larsson, J. Alegret, M. Kall and D. S. Sutherland, *Nano Lett.*, 2007, **7**, 1256.
21 J. Prikulis, P. Hanarp, L. Olofsson, D. Sutherland and M. Kall, *Nano Lett.*, 2004, **4**, 1003.
22 T. Rindzevicius, Y. Alaverdyan, A. Dahlin, F. Hook, D. S. Sutherland and M. Kall, *Nano Lett.*, 2005, **5**, 2335.
23 C. J. Heo, S. H. Kim, S. G. Jang, S. Y. Lee and S. M. Yang, *Adv. Mater.*, 2009, **21**, 1726.
24 J. Homola, *Chem. Rev.*, 2008, **108**, 462.
25 N. L. Rosi and C. A. Mirkin, *Chem. Rev.*, 2005, **105**, 1547.
26 H. Hwang, S. H. Kim and S. M. Yang, *Lab Chip*, 2011, **11**, 87.
27 W. Lee, S. Y. Lee, R. M. Briber and O. Rabin, *Adv. Funct. Mater.*, 2011, **21**, 3424.
28 G. L. Liu and L. P. Lee, *Appl. Phys. Lett.*, 2005, **87**, 074101.
29 L. Y. Wu, B. M. Ross, S. Hong and L. P. Lee, *Small*, 2010, **6**, 503.
30 M. J. Xu, N. Lu, H. B. Xu, D. P. Qi, Y. D. Wang and L. F. Chi, *Langmuir*, 2009, **25**, 11216.
31 S. K. Yang, W. P. Cai, L. C. Kong and Y. Lei, *Adv. Funct. Mater.*, 2010, **20**, 2527.
32 K. Aslan, J. R. Lakowicz and C. D. Geddes, *Appl. Phys. Lett.*, 2005, **87**, 234108.
33 A. G. Brolo, S. C. Kwok, M. G. Moffitt, R. Gordon, J. Riordon and K. L. Kavanagh, *J. Am. Chem. Soc.*, 2005, **127**, 14936.
34 B. Y. Hsieh, Y. F. Chang, M. Y. Ng, W. C. Liu, C. H. Lin, H. T. Wu and C. Chou, *Anal. Chem.*, 2007, **79**, 3487.
35 C. L. Haynes and R. P. Van Duyne, *J. Phys. Chem. B*, 2003, **107**, 7426.
36 J. T. Bahns, Q. T. Guo, J. M. Montgomery, S. K. Gray, H. M. Jaeger and L. H. Chen, *J. Phys. Chem. C*, 2009, **113**, 11190.
37 J. J. Baumberg, T. A. Kelf, Y. Sugawara, S. Cintra, M. E. Abdelsalam, P. N. Bartlett and A. E. Russell, *Nano Lett.*, 2005, **5**, 2262.
38 L. H. Guo, A. R. Ferhan, K. Lee and D. H. Kim, *Anal. Chem.*, 2011, **83**, 2605.
39 Y. J. Huang and D. H. Kim, *Langmuir*, 2011, **27**, 13861.
40 H. A. Atwater and A. Polman, *Nat. Mater.*, 2010, **9**, 205.
41 K. R. Catchpole and A. Polman, *Opt. Express*, 2008, **16**, 21793.
42 V. E. Ferry, L. A. Sweatlock, D. Pacifici and H. A. Atwater, *Nano Lett.*, 2008, **8**, 4391.
43 M. D. Kelzenberg, S. W. Boettcher, J. A. Petykiewicz, D. B. Turner-Evans, M. C. Putnam, E. L. Warren, J. M. Spurgeon, R. M. Briggs, N. S. Lewis and H. A. Atwater, *Nat. Mater.*, 2010, **9**, 239.
44 S. Pillai, K. R. Catchpole, T. Trupke and M. A. Green, *J. Appl. Phys.*, 2007, **101**, 093105.
45 J. A. Schuller, E. S. Barnard, W. S. Cai, Y. C. Jun, J. S. White and M. L. Brongersma, *Nat. Mater.*, 2010, **9**, 193.
46 W. Wang, S. M. Wu, K. Reinhardt, Y. L. Lu and S. C. Chen, *Nano Lett.*, 2010, **10**, 2012.
47 K. R. Catchpole and A. Polman, *Appl. Phys. Lett.*, 2008, **93**, 191113.
48 J. W. Menezes, J. Ferreira, M. J. L. Santos, L. Cescato and A. G. Brolo, *Adv. Funct. Mater.*, 2010, **20**, 3918.
49 K. Nakayama, K. Tanabe and H. A. Atwater, *Appl. Phys. Lett.*, 2008, **93**, 121904.
50 S. M. Yang, S. G. Jang, D. G. Choi, S. Kim and H. K. Yu, *Small*, 2006, **2**, 458.
51 N. D. Denkov, O. D. Velev, P. A. Kralchevsky, I. B. Ivanov, H. Yoshimura and K. Nagayama, *Langmuir*, 1992, **8**, 3183.
52 D. Y. Wang and H. Mohwald, *Adv. Mater.*, 2004, **16**, 244.
53 M. Kondo, K. Shinozaki, L. Bergstrom and N. Mizutani, *Langmuir*, 1995, **11**, 394.
54 M. Trau, S. Sankaran, D. A. Saville and I. A. Aksay, *Nature*, 1995, **374**, 437.
55 L. Y. Wu, B. M. Ross and L. P. Lee, *Nano Lett.*, 2009, **9**, 1956.
56 K. B. Biggs, J. P. Camden, J. N. Anker and R. P. Van Duyne, *J. Phys. Chem. A*, 2009, **113**, 4581.
57 G. H. Chan, J. Zhao, E. M. Hicks, G. C. Schatz and R. P. Van Duyne, *Nano Lett.*, 2007, **7**, 1947.
58 C. L. Haynes and R. P. Van Duyne, *J. Phys. Chem. B*, 2001, **105**, 5599.
59 E. M. Hicks, X. Y. Zhang, S. L. Zou, O. Lyandres, K. G. Spears, G. C. Schatz and R. P. Van Duyne, *J. Phys. Chem. B*, 2005, **109**, 22351.
60 J. Sung, K. M. Kosuda, J. Zhao, J. W. Elam, K. G. Spears and R. P. Van Duyne, *J. Phys. Chem. C*, 2008, **112**, 5707.
61 K. A. Willets and R. P. Van Duyne, *Annu. Rev. Phys. Chem.*, 2007, **58**, 267.
62 X. Y. Zhang, E. M. Hicks, J. Zhao, G. C. Schatz and R. P. Van Duyne, *Nano Lett.*, 2005, **5**, 1503.
63 J. Kim, G. L. Liu, Y. Lu and L. P. Lee, *Opt. Express*, 2005, **13**, 8332.
64 G. L. Liu, Y. Lu, J. Kim, J. C. Doll and L. P. Lee, *Adv. Mater.*, 2005, **17**, 2683.
65 Y. Lu, G. L. Liu, J. Kim, Y. X. Mejia and L. P. Lee, *Nano Lett.*, 2005, **5**, 119.
66 B. M. Ross and L. P. Lee, *Nanotechnology*, 2008, **19**, 275201.
67 S. K. Kim, C. J. Heo, J. Y. Choi, S. Y. Lee, S. G. Jang, J. W. Shim, T. S. Seo and S. M. Yang, *Appl. Phys. Lett.*, 2011, **98**, 233701.
68 D. B. Weibel, W. R. DiLuzio and G. M. Whitesides, *Nat. Rev. Microbiol.*, 2007, **5**, 209.
69 Y. N. Xia and G. M. Whitesides, *Annu. Rev. Mater. Sci.*, 1998, **28**, 153.
70 E. Delamarche, H. Schmid, B. Michel and H. Biebuyck, *Adv. Mater.*, 1997, **9**, 741.
71 T. W. Odom, J. C. Love, D. B. Wolfe, K. E. Paul and G. M. Whitesides, *Langmuir*, 2002, **18**, 5314.
72 K. M. Choi and J. A. Rogers, *J. Am. Chem. Soc.*, 2003, **125**, 4060.
73 H. W. Gao, J. Henzie, M. H. Lee and T. W. Odom, *Proc. Natl. Acad. Sci. U. S. A.*, 2008, **105**, 20146.
74 J. Henzie, E. S. Kwak and T. W. Odom, *Nano Lett.*, 2005, **5**, 1199.
75 J. Henzie, J. Lee, M. H. Lee, W. Hasan and T. W. Odom, *Annu. Rev. Phys. Chem.*, 2009, **60**, 147.
76 J. Henzie, M. H. Lee and T. W. Odom, *Nat. Nanotechnol.*, 2007, **2**, 549.

77 E. S. Kwak, J. Henzie, S. H. Chang, S. K. Gray, G. C. Schatz and T. W. Odom, *Nano Lett.*, 2005, **5**, 1963.
78 M. H. Lee, H. W. Gao, J. Henzie and T. W. Odom, *Small*, 2007, **3**, 2029.
79 N. H. Mack, J. W. Wackerly, V. Malyarchuk, J. A. Rogers, J. S. Moore and R. G. Nuzzo, *Nano Lett.*, 2007, **7**, 733.
80 V. Malyarchuk, F. Hua, N. H. Mack, V. T. Velasquez, J. O. White, R. G. Nuzzo and J. A. Rogers, *Opt. Express*, 2005, **13**, 5669.
81 M. E. Stewart, C. R. Anderton, L. B. Thompson, J. Maria, S. K. Gray, J. A. Rogers and R. G. Nuzzo, *Chem. Rev.*, 2008, **108**, 494.
82 J. M. Yao, A. P. Le, S. K. Gray, J. S. Moore, J. A. Rogers and R. G. Nuzzo, *Adv. Mater.*, 2010, **22**, 1102.
83 N. Feth, C. Enkrich, M. Wegener and S. Linden, *Opt. Express*, 2007, **15**, 501.
84 C. H. Liu, M. H. Hong, H. W. Cheung, F. Zhang, Z. Q. Huang, L. S. Tan and T. S. A. Hor, *Opt. Express*, 2008, **16**, 10701.
85 J. Li, H. Iu, D. Y. Lei, J. T. K. Wan, J. B. Xu, H. P. Ho, M. Y. Waye and H. C. Ong, *Appl. Phys. Lett.*, 2009, **94**, 183112.
86 J. Li, H. Iu, J. T. K. Wan and H. C. Ong, *Appl. Phys. Lett.*, 2009, **94**, 033101.
87 Q. Z. Li and G. P. Wang, *Opt. Express*, 2010, **18**, 14123.
88 J. H. Lee, Q. Wu and W. Park, *Opt. Lett.*, 2009, **34**, 443.
89 X. Zhang, M. Theuring, Q. Song, W. D. Mao, M. Begliarbekov and S. Strauf, *Nano Lett.*, 2011, **11**, 2715.
90 J. Lu, D. Chamberlin, D. A. Rider, M. Z. Liu, I. Manners and T. P. Russell, *Nanotechnology*, 2006, **17**, 5792.
91 H. Acharya, J. Sung, B. H. Sohn, D. H. Kim, K. Tamada and C. Park, *Chem. Mater.*, 2009, **21**, 4248.
92 P. A. Mistark, S. Park, S. E. Yalcin, D. H. Lee, O. Yavuzcetin, M. T. Tuominen, T. P. Russell and M. Achermann, *ACS Nano*, 2009, **3**, 3987.
93 Y. Wang, M. Becker, L. Wang, J. Q. Liu, R. Scholz, J. Peng, U. Gosele, S. Christiansen, D. H. Kim and M. Steinhart, *Nano Lett.*, 2009, **9**, 2384.
94 D. Choi, Y. Choi, S. Hong, T. Kang and L. P. Lee, *Small*, 2010, **6**, 1741.
95 M. Schierhorn, S. J. Lee, S. W. Boettcher, G. D. Stucky and M. Moskovits, *Adv. Mater.*, 2006, **18**, 2829.
96 S. Shukla, K. T. Kim, A. Baev, Y. K. Yoon, N. M. Litchinitser and P. N. Prasad, *ACS Nano*, 2010, **4**, 2249.
97 M. Shaban, H. Hamdy, F. Shahin and S. W. Ryu, *J. Nanosci. Nanotechnol.*, 2010, **10**, 3034.
98 H. H. Wang, C. Y. Liu, S. B. Wu, N. W. Liu, C. Y. Peng, T. H. Chan, C. F. Hsu, J. K. Wang and Y. L. Wang, *Adv. Mater.*, 2006, **18**, 491.
99 W. A. Murray and W. L. Barnes, *Adv. Mater.*, 2007, **19**, 3771.
100 W. Kubo and S. Fujikawa, *Nano Lett.*, 2011, **11**, 8.
101 A. J. Haes, W. P. Hall, L. Chang, W. L. Klein and R. P. Van Duyne, *Nano Lett.*, 2004, **4**, 1029.
102 J. McPhillips, A. Murphy, M. P. Jonsson, W. R. Hendren, R. Atkinson, F. Hook, A. V. Zayats and R. J. Pollard, *ACS Nano*, 2010, **4**, 2210.
103 C. L. Haynes, A. D. McFarland and R. P. Van Duyne, *Anal. Chem.*, 2005, **77**, 338a.
104 K. Kneipp, *Phys. Today*, 2007, **60**, 40.
105 M. Fleischm, P. J. Hendra and Aj. Mcquilla, *Chem. Phys. Lett.*, 1974, **26**, 163.
106 Y. H. Sun, K. Liu, J. Miao, Z. Y. Wang, B. Z. Tian, L. N. Zhang, Q. Q. Li, S. S. Fan and K. L. Jiang, *Nano Lett.*, 2010, **10**, 1747.
107 H. Ko and V. V. Tsukruk, *Small*, 2008, **4**, 1980.
108 N. Ji, W. D. Ruan, C. X. Wang, Z. C. Lu and B. Zhao, *Langmuir*, 2009, **25**, 11869.
109 V. Giannini, A. I. Fernandez-Dominguez, S. C. Heck and S. A. Maier, *Chem. Rev.*, 2011, **111**, 3888.
110 N. N. Lal, B. F. Soares, J. K. Sinha, F. Huang, S. Mahajan, P. N. Bartlett, N. C. Greenham and J. J. Baumberg, *Opt. Express*, 2011, **19**, 11256.
111 W. A. Luhman, S. H. Lee, T. W. Johnson, R. J. Holmes and S. H. Oh, *Appl. Phys. Lett.*, 2011, **99**, 103306.